Au and NiO nanocrystals doped into porous sol-gel SiO2 films and the effect on optical CO detection

Buso, D.; Guglielmi, M.; Martucci, A.; Mattei, G.; Mazzoldi, P.; Sada, C.; Post, M. L.

Publisher's version / Version de l'éditeur:
https://doi.org/10.1088/0957-4484/17/10/001
Nanotechnology, 17, pp. 2429-2433, 2006

INSTITUTE OF PHYSICS PUBLISHING NANOTECHNOLOGY
Nanotechnology **17** (2006) 2429–2433 doi:10.1088/0957-4484/17/10/001

Au and NiO nanocrystals doped into porous sol–gel SiO_2 films and the effect on optical CO detection

D Buso[1], M Guglielmi[1], A Martucci[1], G Mattei[2], P Mazzoldi[2], C Sada[2] and M L Post[3]

[1] Dipartimento di Ingegneria Meccanica–Settore Materiali, Università di Padova, via Marzolo, 9, I-35131 Padova, Italy
[2] Dipartimento di Fisica, Università di Padova, via Marzolo 8, I-35131 Padova, Italy
[3] Institute for Chemical Process and Environmental Technology, National Research Council of Canada, 1200 Montreal Road, Ottawa, ON, K1A 0R6, Canada

Received 7 February 2006, in final form 17 March 2006
Published 24 April 2006
Online at stacks.iop.org/Nano/17/2429

Abstract
Thin-film composites comprised of NiO and NiO/Au nanoparticles in a porous SiO_2 matrix have been prepared using the sol–gel technique. When at elevated temperatures (200 °C $< T <$ 350 °C) and exposed to carbon monoxide, the films undergo reversible changes in optical transmittance at wavelengths in the visible–near IR region. For NiO composite films heated at 330 °C and exposed to 1% CO in air, there is an increase in transmittance which approaches 2–4% over most of the visible range. For NiO/Au composite films the transmittance increase exhibits a wavelength dependence, with a maximum change which is close to 6% at $\lambda \approx 630$ nm and which is close to zero in the Au plasmon resonance range ($\lambda \approx 550$ nm).

1. Introduction

Materials that show a detectable and reversible change of their optical absorption properties in the presence of certain gaseous species have considerable potential applications as opto-chemical gas sensors. Some of the advantages of optical devices over conventional conductometry-based gas sensors lie in their high resistivity to electromagnetic noise, fire resistance, inactivity in flammable environments and also capability for remote control and information transfer through optical fibre networks [1, 2]. Furthermore new potential applications in multi-gas detection can be achieved using differences in the intensity, wavelength, phase and polarization of the output light signal [3]. Kobayashi *et al* [4] first observed that thin films of NiO, Co_3O_4 and MnO_3 showed reversible decreases in the visible–NIR absorption induced by CO at temperatures around 250–350 °C. The absorbance change was then associated with a decrease in positive hole density on the oxide surface during catalytic CO oxidation. Later it was established that the introduction of small Au particles in the films enhanced the sensitivity towards the same gases [5, 6] or in some cases induced it where previously no response had been present [7]. The current work demonstrates the enhanced optical gas sensing effect which is induced by the introduction of Au particles into a porous sol–gel silica matrix doped with NiO nanocrystals as compared to the Au undoped one. To the authors' knowledge such an enhancement has not been previously observed in sol–gel silica films doped with noble metals together with transition metal oxides. Thin films obtained via the sol–gel method are a promising matrix support for active materials in gas sensing applications because of their high and tunable inner porosity, that can provide specific surface values up to 600 $m^2\ g^{-1}$ [8].

2. Experimental details

The synthetic sol–gel route adopted for the preparation of both SiO_2–NiO and SiO_2–NiO–Au films is shown schematically in figure 1.

The precursor solution for the silica matrix was made by mixing tetraethoxy silane (TEOS), methyl-triethoxy silane (MTES), H_2O, HCl in EtOH according to molar ratios TEOS:MTES:H_2O:HCl:EtOH = 1:1:4:0.02:4. The NiO precursor solution was made by mixing $NiCl_2{\cdot}6H_2O$ in EtOH in the presence of *N*-[3-(trimethoxysilyl)propyl]-ethylenediamine (DAEPTMS) keeping the molar ratio of

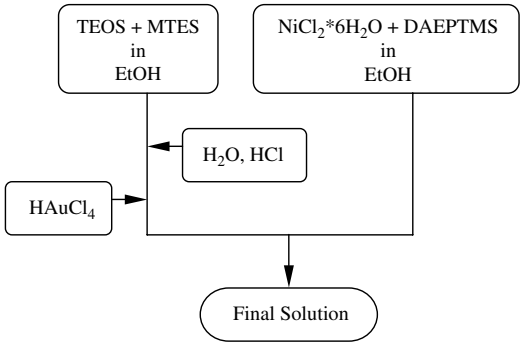

Figure 1. Synthetic route followed for the synthesis of the sol–gel solution.

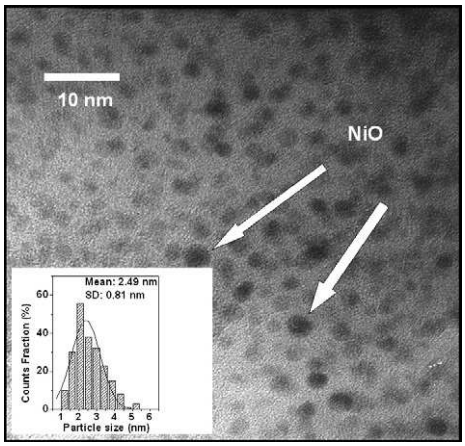

Figure 2. TEM image of the SiO_2–NiO film annealed at 500 °C for 30 min. Inset: size distribution of the NiO nanoparticles.

Ni:DAEPTMS = 1. The double aminic groups of DAEPTMS coordinate the Ni^{2+} cations in the solution while the silanic group ensures the homogeneous dispersion of cations distributed inside the final SiO_2 network. The solution for the production of SiO_2–NiO films was obtained by mixing the two precursor sols in the due amount to obtain a final composite with a SiO_2:NiO ratio of 3:2 (60% SiO_2–40% NiO molar). For the Au doping, $HAuCl_4 \cdot 3H_2O$ was used as the metallic gold precursor and added directly in the matrix solution according to a Ni:Au = 5:1 molar ratio. The two precursor sols were then mixed together to obtain the final batch.

Films were deposited on quartz glass substrates via the *dip-coating* technique using a withdrawing speed of 100 cm min^{-1} at 23 °C and controlled relative humidity (RH% = 25%). Thermal annealing of the films was performed in air at 500 °C for 30 min.

Structural and compositional characterization was performed at CNR-IMM (Bologna, Italy) on cross-sectional samples of the composite films. Measurements were taken with a field-emission FEI TECNAI F20 SuperTwin FEG-(S)TEM microscope operating at 200 kV and equipped with an EDAX energy-dispersive x-ray spectrometer (EDS) for compositional analysis and a Gatan 794 Multiple Scan Camera, allowing digital image recording on a 1024 × 1024 pixel CCD array. Scanning TEM (STEM) analysis coupled with EDS allowed compositional analysis on single clusters by means of line scans with an electron probe resolution of 1 nm FWHM.

SIMS measurements were carried out by means of an IMS 4f mass spectrometer (Cameca, Padova, Italy) using a 10 kV Cs^+ primary beam and by negative secondary ion detection (the sample potential was fixed at +4.5 kV) with a final impact energy of 14.5 keV. The SIMS spectra were obtained in ultrahigh vacuum conditions at a different primary beam intensity (15 nA) rastering over a nominally 125 × 125 μm^2 area. The beam blanking mode was used to improve the depth resolution, by interrupting the sputtering process during magnet stabilization periods. The dependence of the erosion speed on the matrix composition was taken into account by measuring the erosion speed at various depths for each sample. The erosion speed was then evaluated by measuring the depth of the erosion crater at the end of each analysis by means of a Tencor Alpha Step profilometer with a maximum uncertainty of a few nanometres. The measurements were performed in a high mass resolution configuration to avoid mass interference artefacts, and the charge build-up while profiling the insulating samples was compensated by an electron gun without any need to cover the surface with a metal film.

Optical sensor functionality was studied by performing optical absorbance/transmittance measurements over the wavelength range 350 nm < λ < 800 nm with sample films mounted on a heater in a custom built gas flow cell. Transmission data were recorded with a Varian Cary1E spectrophotometer with films heated at temperatures between room temperature and 350 °C and CO concentrations ranging from 10 to 10 000 ppm in dry air. The substrate size for these measurements was approximately 1 cm × 2 cm and the incident spectrophotometer beam was normal to the film surface and covered a 6 mm × 1.5 mm section area.

3. Results and discussion

3.1. Morphology of the films

Figure 2 shows a TEM image of the SiO_2–NiO composite film.

Previous work reported that the dark contrast aggregates visible in the TEM image are crystalline NiO clusters [9]. The NiO crystals visible in figure 2 are homogeneously dispersed inside the SiO_2 matrix. The SIMS measurements also showed a homogeneous distribution of Ni and O species through the whole SiO_2–NiO film thickness [9].

The mean particle diameter evaluated from figure 2 was found to be 2.5 ± 0.8 nm (average diameter ± standard deviation of the experimental size distribution) as seen from the size distribution diagram inset in figure 2.

Detailed HRTEM analysis was conducted for the SiO_2–NiO–Au film (figure 3) to unequivocally determine the nature of the crystalline aggregates that were observed, and concluding that nucleation and growth of NiO crystalline clusters took place beside metallic gold formation: in figure 3 some NiO particles are clearly visible near to an Au cluster. Lattice planes of both aggregates are easily recognizable, and the high resolution of the image permitted assigning them to the $Au_{\langle 111 \rangle}$ fcc plane ($d_{\langle 111 \rangle}$ = 0.236 nm) and $NiO_{\langle 200 \rangle}$ fcc

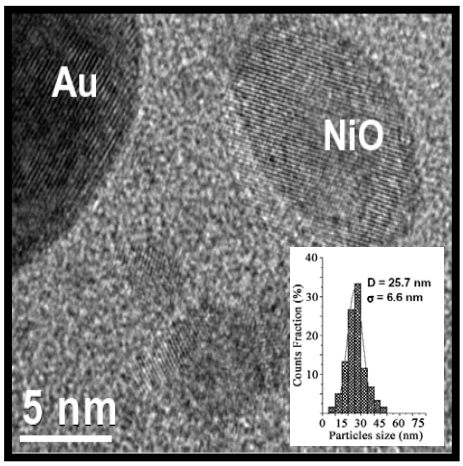

Figure 3. High resolution TEM (HRTEM) image of the SiO_2–NiO–Au film heated at 500 °C for 30 min. One gold and one NiO nanocrystal are visible showing ⟨111⟩ and ⟨200⟩ lattice planes respectively. Inset: size distribution of gold nanoparticles.

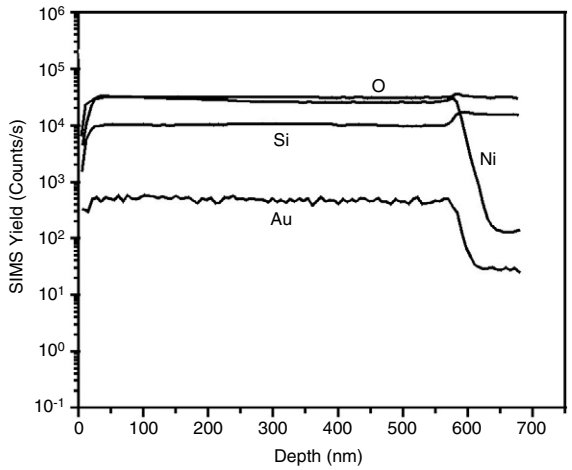

Figure 4. SIMS data of an SiO_2–NiO–Au film showing depth profiles of Si, Ni, O and Au species.

structure plane ($d_{\langle 200\rangle} = 0.207$ nm). Additionally, in a very few clusters a periodicity of 0.201 nm was also found which can be attributed to the ⟨111⟩ planes of an fcc Ni phase[4]. The distinction between Au and NiO aggregates is also confirmed by EDS-STEM analysis on both clusters as shown in figure 3: no Au EDS signal is obtained when focusing the beam onto the cluster giving $NiO_{\langle 200\rangle}$ lattice fringes, whereas it is dominant when focusing on the other cluster. Size evaluation showed a bi-modal distribution of clusters: a first distribution of small particles (NiO) represented by spherical clusters with size of about 5 nm, and a second distribution of particles with a more elongated shape in the region of 25 nm, that is associated with Au aggregates. Statistically, the major axis of the latter Au elongated particles lies parallel to the film surface. The nanocluster size (averaged over the two main axes) for this second population is 26 ± 7 nm. The SIMS data reported in figure 4 demonstrate that also in the case of SiO_2–NiO–Au films both Ni and Au species are uniformly distributed through the whole film thickness.

[4] Powder Diffraction File Nos: 04-0784 (Au), 78-0643 (NiO); 04-0850 (Ni).

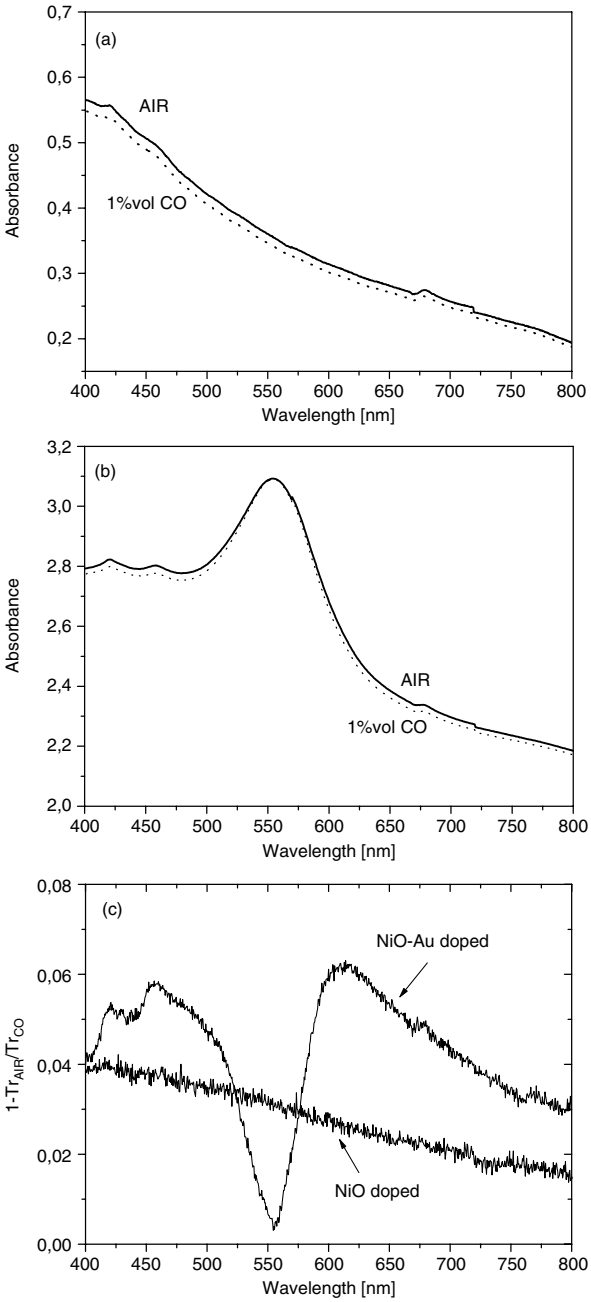

Figure 5. Absorption spectra of the films at an operative temperature of 330 °C. (a) SiO_2–NiO film in dry air (solid line) and after exposure to 1 vol% CO (dotted line). (b) SiO_2–NiO–Au film in dry air (solid line) and after exposure to 1 vol% CO (dotted line). (c) Comparison of the relative change in the transmittance $\Delta \mathrm{Tr}\,\% = 1 - \mathrm{Tr}_{\mathrm{AIR}}/\mathrm{Tr}_{1\%\mathrm{CO}}$ for both films at an operative temperature of 330 °C.

3.2. Functional characterization as a gas sensor

Film functionality in gas detection was tested using a custom built gas flow chamber that allows acquisition of absorbance spectra in an atmospheric conditioned environment. Figures 5(a) and 4(b) show the absorbance obtained for the

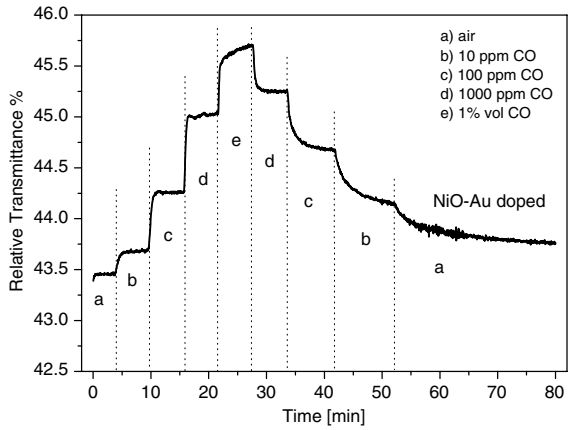

Figure 6. Temporal response for SiO_2–NiO–Au films as a function of the CO concentration in air. Measurements at an operative temperature of 330 °C and $\lambda = 690$ nm.

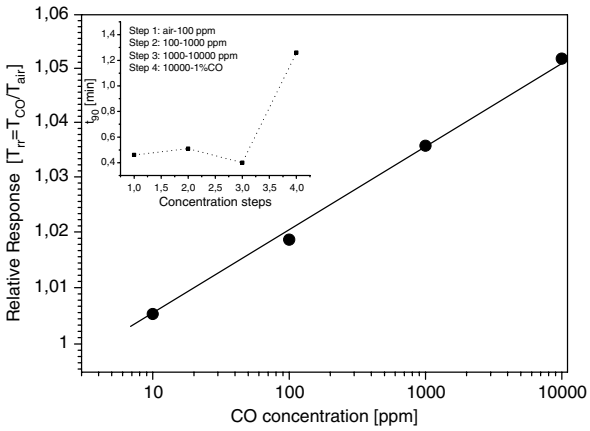

Figure 7. Log of relative response $T_{rr} = [Tr_{CO}/Tr_{air}]$ versus log of gas concentration and (inset) response rate (t_{90}) versus gas concentration of the SiO_2–NiO–Au film.

SiO_2–NiO and SiO_2–NiO–Au films when exposed sequentially to either air or 1% CO at 330 °C. This operative measurement temperature was chosen according to previous characterizations to ensure adequate reaction kinetics [10].

SiO_2–NiO film (figure 5(a)) showed a clear absorbance decrease over the whole visible region when exposed to 1% CO. Also the SiO_2–NiO–Au film (figure 5(b)) showed an overall decrease in optical absorption when exposed to 1% CO at the same operating temperature.

To better compare the sensitivity of the two materials to 1% CO exposure at 330 °C, figure 5(c) shows ΔTr%, the relative variation in transmittance, defined as $\Delta Tr\% = 1 - Tr_{AIR}/Tr_{1\%CO}$. For the SiO_2–NiO film ΔTr% increases linearly from high to lower wavelengths, demonstrating a slight wavelength dependence and reaching its maximum value around 410–420 nm ($\Delta Tr\%_{max}$ of about 4%). For the SiO_2–NiO–Au film ΔTr% exhibits a non-monotonic behaviour reaching its maximum between 620 and 640 nm, with a $\Delta Tr\%_{max}$ of about 6% that demonstrates an effective enhancement in CO detection induced by gold clusters. Furthermore the wavelength dependence of ΔTr% values is extremely marked for the SiO_2–NiO–Au film. A strong suppression of the CO induced absorbance variation is detectable at wavelengths corresponding to the plasmonic resonance frequencies of the Au clusters, the same effect having been being observed previously in NiO–Au films [6] and Au–Co_3O_4 composite films [11] by other authors. One possible explanation could be provided by studies conducted by Matsubara *et al* [12] on thin metal films deposited on a transparent metal oxide. Those authors report that the evanescent wave from the metal oxide was effectively absorbed by the surface plasmon of the thin metal film at the interface. This suggests that the absorbance decrease of NiO induced by CO might be compensated by the plasmon band absorption of the small Au particles. As already pointed out by Ando *et al* for NiO–Au films [6] and Au–Co_3O_4 composite films [11] different gases (i.e. CO and H_2) give different wavelength dependences of ΔTr% which could be exploited for multi-gas detection at multiple wavelengths.

Figure 6 shows the temporal response characteristics of the SiO_2–NiO–Au film when exposed to different concentrations of CO in air, in a stepwise manner, for the range 10 ppm to 1 vol% CO. These data were obtained at the same operating temperature ($T = 330$ °C) as those reported in previous figures. The wavelength used for these measurements was $\lambda = 690$ nm. For 1% CO exposure, the overall transmittance change is ∼2.2% at $\lambda = 690$ nm and the shape of the transmittance steps shows a good signal reversibility (i.e. recovery of the signal baseline after a change of CO concentration) in the case of high CO concentrations, while at lower gas concentrations the exponential baseline recovery takes a longer time.

Figure 7 summarizes the characteristics of the SiO_2–NiO–Au film in terms of two main sensing parameters: sensitivity and response rate. On defining the film relative response as the ratio $T_{rr} = [Tr_{CO}/Tr_{air}]$ of the sensor transmittance in test gas (Tr_{CO}) to that in air (Tr_{air}), and plotting the relative response (T_{rr}) and gas concentration logarithmically, the relationship is linear, as shown in figure 7.

The inset of figure 7 shows the value of the response rate of SiO_2–NiO–Au film calculated from data of figure 6 and indicated as t_{90}. The value of t_{90} is one of the parameters that are commonly adopted to provide the functional description of industrial sensors and it indicates the amount of time that the sensor requires to reach 90% of the equilibrium signal after a gas concentration variation. The reported values of the response time (mean value around 30 s) are comparable with t_{90} for most of the industrial CO sensors which was found to be generally in the range 1–150 s [13].

3.3. CO detection mechanism

A correlation between film porosity and gas detection functionality found in previously reported work [10] has demonstrated that in the three-step process of gas detection ((i) diffusion of target gas inside the film, (ii) reaction over the active surface of metal oxide, (iii) diffusion of reaction products outside of the film) the film porosity plays a key role in maximizing the diffusion steps rates in order to leave the reaction rate as the rate determining step for the overall detection process. The films described here underwent a thermal treatment that results in a residual porosity that is

suitable for a quick and consistent gas response at an operating temperature of 330 °C [10]. At temperatures lower than 200 °C no relevant absorbance variation was detected even for 1 vol% CO, indicating that the CO to CO_2 conversion is thermally promoted at temperatures that are higher than those observed for catalytic oxidation of CO to CO_2 with powdered catalysts (down to −70 °C) [14]. The observed difference in operative temperature reflects differences in reaction pathways for CO sensing and catalytic CO oxidation as are also observed for Au particles deposited onto NiO films [14]. The commonly accepted reaction pathway for CO sensing is the so-called 'CO-sensitive charge carrier density change', which comprises the formation and decomposition of carbonate-like species such as CO_3^{2-} at the oxide surface. This process causes a decrease in the positive hole density according to [15]

$$CO + 2O^{2-} + 2V_O^{2+} \rightarrow CO_3^{2-} + 2V_O^{+}$$

where V_O^{2+} is a divalent oxygen vacancy and V_O^{+} is a monovalent oxygen vacancy. This reaction is known to be accelerated only at temperatures above 100 °C [11].

To explain the increased sensitivity of the sensor when small Au particles are combined with transition metal oxides, two types of enhancing effect have been proposed [16]. *Type 1* effects are related to an increased catalytic activity promoted by gold, closely associated with the catalytic activity of the Au–transition metal oxide composite [14]. In *Type 2* effects the enhancement arises from the plasmon absorption change of Au particles, and it is not directly related to catalytic CO oxidation. Plasmon resonance frequencies are strongly influenced by the physical properties of the surrounding material, such as dielectric constants. A gas induced variation of these properties would affect both the wavelength and the shape of the plasmon absorption band of gold particles, as observed in Au–Co_3O_4 [11] and Au–CuO [16] films. In the case of SiO_2–NiO–Au film (figure 5(b)) no variation in either wavelength or shape of the plasmon band was observed, so a *Type 1* enhancing effect can reasonably be proposed as the working mechanism that explains the sensitivity increase observed in the Au doped films described here.

4. Conclusions

Thin sol–gel silica films doped with nanoparticles of NiO and NiO–Au showed variations of their optical absorbance when exposed to CO in dry air at 330 °C. The absorbance change is reversible and the films are CO sensitive at gas concentrations down to 10 ppm. The introduction of Au nanoparticles in the SiO_2–NiO film is effective in CO detection enhancement. This suggests that the Au doping increases the catalytic activity of the material in the CO oxidative mechanism which results in the gas detection. Furthermore the presence of Au induces a strong CO sensitivity suppression at wavelengths corresponding to the plasmon peak resonance of the noble metal, this giving the opportunity to test these materials in multi-gas sensing.

Acknowledgment

This work was supported by MURST within a 'Progetto di Ateneo No CPDA042175' Project of the Padova University.

References

[1] Educhi K 1992 Optical gas sensors *Gas Sensors* ed G Sberveglieri (Dordrecht: Kluwer–Academic) pp 307–28
[2] Seiz W R 1984 Chemical sensors based on fiber optics *Anal. Chem.* **56** 16A
[3] Ando M, Kobayashi T and Haruta M 1997 Combined effects of small gold particles on the optical gas sensing by transition metal oxides films *Catal. Today* **36** 135
[4] Kobayashi T, Haruta M, Sano H and Delmon B 1990 Optical detection of CO in air through catalytic chromism of metal-oxide thin films *Proc. 3rd Int. Mtg on Chemical Sensors (Cleveland)* pp 318–21
[5] Kobayashi T, Haruta M and Ando M 1993 Enhancing effect of gold deposition in the optical detection of reducing gases in air by metal oxide thin films *Sensors Actuators* B **13/14** 545
[6] Ando M, Kobayashi T and Haruta M 1994 Enhancement in the optical CO sensitivity of NiO film by the deposition of ultrafine gold particles *J. Chem. Soc. Faraday Trans.* **90** 1011
[7] Ando M, Kobayashi T and Haruta M 1995 Optical CO detection by use of CuO/Au composite films *Sensors Actuators* B **24/25** 851
[8] Brinker C J and George W 1990 *Scherer Sol–gel Science: the Physics and Chemistry of Sol–Gel Processing* (Boston: Academic)
[9] Martucci A, Buso D, De Monte M, Guglielmi M, Cantalini C and Sada C 2004 Nanostructured sol–gel silica thin films doped with NiO and SnO_2 for gas sensing applications *J. Mater. Chem.* **14** 2889
[10] Martucci A, Pasquale M, Guglielmi M, Post M and Pivin J C 2003 Nanostructured SiO_2–NiO sol–gel films with enhanced optical CO gas sensitivity *J. Am. Ceram. Soc.* **86** 1638
[11] Ando M, Kobayashi T, Iijima S and Haruta M 1997 Optical recognition of CO and H_2 by use of gas-sensitive Au–Co_3O_4 composite films *J. Mater. Chem.* **7** 1779
[12] Matsubara K, Kawata S and Minami S 1988 A compact surface plasmon resonance sensor for measurement of water in process *Appl. Spectrosc.* **42** 1375
[13] See for example: CEA Instruments, Inc.-Online Catalog-Page 2; ENVCO-Series 500 Ozone Monitor; IRceL® Miniature Infrared Gas Sensors; Model PT295-LEL Combustible Gas Sensor- Pem-Tech, Inc; Ist-Aim Instruments, Page 3
[14] Haruta M, Yamada N, Kobayashi T and Iijima S 1989 Gold catalysts prepared by coprecipitation for low-temperature oxidation of hydrogen and carbon monoxide *J. Catal.* **115** 301
[15] Boccuzzi F, Chiorino A, Tsubota S and Haruta M 1995 An IR study of CO-sensing mechanism on Au/ZnO *Sensors Actuators* B **24/25** 540
[16] Ando M, Kobayashi T, Iijima S and Haruta M 2003 Optical CO sensitivity of Au–CuO composite film by use of the plasmon absorption change *Sensors Actuators* B **96** 589